屏蔽二型類星體的塵埃與其周圍星系環境的研究

徐麗婷、陳林文
國立台灣師範大學地球科學系

摘要

富含星際塵埃的二型類星體在星系演化上可能扮演著十分重要的角色，它所處的演化階段可能正是決定該活躍星系所釋放出來的能量將主要是來自於中心大質量黑洞的吸積作用或是恆星遽增的關鍵時期。在本研究中，我們由史隆數位巡天計畫的可見光資料庫中選出一型與二型類星體，對此兩者作多波段的統計研究與比較。我們的分析結果顯示這兩種類型的類星體不論在1.4 GHz電波波段的光度函數上，亦或在可見光的Δ(g-i)色指數上都有所不同。然而在他們周圍1.5 Mpc半徑的星系環境上卻沒有太明顯的差別。此外，我們還利用ROSAT巡天觀測中的資料，計算出這些二型類星體本身的中性氫原子的柱密度下限，同時結合其可見光色指數來討論屏蔽物質的本質與類星體演化的關係。

Obscuration in Type 2 QSOs and Their Environments

Li-Ting Hsu, Lin-Wen Chen
Department of Earth Sciences, National Taiwan Normal University, Taipei, Taiwan.

Abstract

Type 2 QSOs are possibly at a key stage of galaxy evolution that could reveal the process to decide whether the output power of an active galaxy is in an accretion dominated or starburst dominated phase. In this work, we carry out a statistical analysis of several multiwavelength properties of optically selected type 2 QSOs to compare their characteristics with those of type 1 QSOs. The type 1 QSO and type 2 QSO samples are from the released catalogues based on SDSS database. Our analysis results show that the 2 types of QSOs have systematic differences in their radio luminosity functions at 1.4 GHz, optical photometry, and dust obscuration indicated by the relative SDSS (*g*-*i*) color. However there is no indication of difference in environments, namely, the number density of galaxies in neighboring 1.5 Mpc radius region. Furthermore, we derive the lower limit of neutral hydrogen column density of selected bright type 2 QSOs using the ROSAT All Sky Survey (RASS) data, and combine the result with their relative (*g*-*i*) color to discuss the nature of the obscuring material, as well as its implication to QSO evolution.

關鍵字 (Keywords)：類星體 (quasar)、活躍星系 (active galaxy)、星系演化 (galaxy evolution)

Received : 2009.11.02; accepted: 2009.12.10

1. Introduction

Type 2 QSOs (QSO2) are defined as intrinsically luminous ($L_{2\text{-}10\ keV} > 10^{44}$ erg s^{-1}) active galactic nuclei (AGN) with large hydrogen column densities ($N_H > 10^{22}$ cm^{-2}) (e.g., Gilli et al. 2001; Norman et al. 2002; Stern et al. 2002, Ptak et al.2006; Fiore et al.2009), such strong obscuration is supposedly in both optical and soft X-ray bands. According to the classical unification model of AGN, all AGN have the same intrinsic spectrum and evolution (Comastri et al. 1995), except the obscured ones lack broad optical emission lines due to orientation effects and dust torus. Based on this assumption, Zakamska et al. (2003) have selected several hundreds of QSO2 from the Sloan Digital Sky Survey (SDSS) database using the properties of their narrow emission line originating outside the obscuring torus.

However, Wilman & Fabian (1999) have shown signs of a large population of obscured AGN when modeling Hard X-ray background (XRB). The absorption (neutral hydrogen column density $N_H > 10^{22}$ cm^{-2}) occurs in 90 percent of unresolved XRB sources and heavy absorption ($N_H > 10^{24}$ cm^{-2}) in 30~50 percent of XRB. Such high absorbed fractions cannot be accounted by a thin disc or by the standard torus of unified models. This model also suggests that the high obscuration phase occurs only during the growing phase, and finally becomes powerful unobscured AGNs. More recently, Martínez-Sansigre et al. (2006a) proposed that the dust in QSO2 can be explained by 'host-obscured' or 'torus-obscured'.

In this work, we use the radio, optical, and soft-X-ray data to investigate the evolutionary stage of QSO2 and the properties of obscuring material. As the environments can play an important role in boosting AGN activities and evolution of host galaxies (e.g., Yee & Ellingson 1993; Poggianti et al. 2006; Strand et al. 2008), we also measure the galaxy density around type 1 and type 2 QSOS as an indicator of their evolutionary stages. We therefore combine radio luminosities, optical colors, and environments of QSOs to investigate the connection between type 1 and type 2 QSOs. The intrinsic X-ray luminosity of obscured quasars is derived from observed SDSS [OIII] luminosity via a soft X-ray luminosity - [OIII] relation proposed by Shen et al. (2006). Compared the estimated X-ray luminosity with the flux limit of ROSAT All Sky Survey (RASS), the lower limit of neutral hydrogen column density toward each QSO2 can be obtained; finally, we use relative SDSS *g-i* to discuss the dust property in QSO2.

Throughout this paper, values of $H_0 = 70$ km $s^{-1}Mpc^{-1}$, $\Omega_M = 0.3$, $\Omega_\Lambda = 0.7$ are adopted, [OIII] luminosities are expressed as $L_{[OIII]}$ in

units of solar luminosities ($L_{\odot} = 3.86 \times 10^{33}$ erg s^{-1}).

2. Sample Selection

We selected 887 QSO2 from Reyes et al. (2008) catalogue originally derived from Sloan Digital Sky Survey (SDSS) Data Release sixth spectroscopic database. The selection criteria of the catalogue include high ionization, narrow emission lines without underlying broad components and with line ratios characteristic of non-stellar ionizing radiation (Zakamska et al. 2003). These QSO2 are also restricted to $z <$ 0.83 so that the [OIII]5008 line is present in all spectra which cover 3800–9200 Å, and the line diagnostic criteria from Kewley et al. (2001) are used to distinguish QSO2 from star-forming galaxies and narrow-line Seyfert galaxies. The [OIII]5008 line of these QSO2 samples are also corrected for Galactic extinction. To systematically compare QSO2 with type 1 QSOs (QSO1) in different luminosity ranks, we also select QSO1 data from the following three catalogues: (1) SDSS photometric quasar catalogue (Schneider et al. 2007); (2) SDSS spectroscopic quasar catalogue (Ofek et al. 2007); and (3) PG quasars (Jester et al. 2005).

The photometric quasar (QSO_{PH}) samples have luminosities $Mi < -22$ with at least one emission line with FWHM larger than 1000 km s^{-1}; the spectroscopic quasars (QSO_{SP}) have *i*-band magnitude brighter than 19.0; and the PG quasars (QSO_{PG}) are selected from SDSS Data of the Palomar-Green (PG) Bright Quasar Survey (BQS) with $i < 15$.

To study the environment of obscured and unobscured QSOs, we select galaxies around central QSOs in 1.5 Mpc (typical size of a galaxy cluster) from SDSS seventh Data Release. The redshift of the selected galaxies is restricted to below 0.83 as same as that of QSO2 and the redshift range of surrounding galaxies centered on each QSO2 is about 0.1 (Strand et al. 2008). Taking the completeness of SDSS source detection into account, we only count galaxies more luminous than –21.4 in *r*-band to correct the selection effect as the limiting flux is $r = 22.2$ and our most distant QSO2 is up to redshift = 0.83.

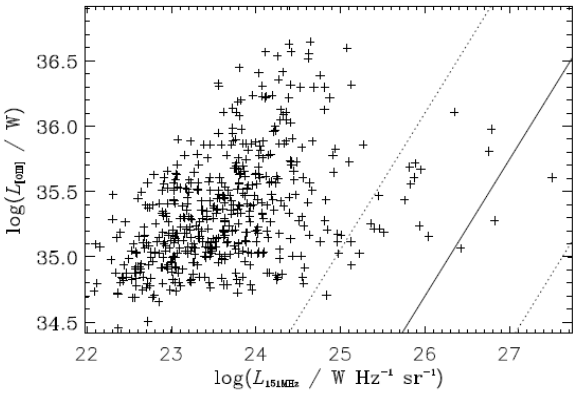

Fig. 1: Correlation between L_{151} and $L_{[OIII]}$ for type 2 QSOs (cross symbols). The solid line indicates the best fit to the radio-loud samples in Grimes et al. (2004), which follows the relationship:
$\log (L_{[OIII]}) = (3.4 \times 10^7 \times L_{151}^{1.045})$.
The dotted lines represent the region in which radio-loud sources are expected to reside.

3. Data Analysis and Result

3.1. Analysis of Radio data

To investigate the radio "loudness" of QSO2s, we adopt the criterion from McCarthy (1993) which is originally for radio galaxies and is based on ratios of 151 MHz luminosity (L_{151}) to $L_{[OIII]}$ (Fig. 1). The narrow component of [OIII] emission line is most likely from

AGN narrow line regions, and it is therefore broadly independent of the jet-axis orientation (Grimes et al. 2004), and less contaminated by star lights in the host galaxy (Zakamska et al. 2003).

We have 531 QSO2 with FIRST 1.4 GHz flux, and convert the 1.4 GHz flux to 151 MHz luminosity with an assumed power-law spectral energy distribution (SED) and a spectral index α=0.8 (Martínez-Sansigre et al. 2006a). Compared with the radio-loud QSO1 in Grimes et al. (2004), these QSO2 have fainter L_{151} by a factor of 100 which are similar to the result of Infrared-radio-selected QSO2 from Martínez-Sansigre et al. (2006a). We set

$$p = \log(L_{[OIII]}) - (3.4 \times 10^7 \times L_{151}^{1.045}) \qquad (1)$$

(Hsu & Chen 2010) to indicate the offset from the best fit line of radio-loud (p=0) samples (Fig. 2). We find 25 out of 531 available QSO2 are radio- loud, and this fraction is also smaller than that of QSO1 by a factor of about 2 (Green et al 2009).

3.2. Environments of QSO1 and QSO2

To test whether the origin of QSO obscuration is environment-driven, we have made a comparison of QSO1 and QSO2 environments. We select galaxies over a cluster-scale region around central QSOs (1.5 Mpc radius) from SDSS seventh Data Release, and subsequently combine the data with 1.4 GHz luminosity and $\Delta(g\text{-}i)$ (which can indicate the dust property of QSOs) for further analysis.

Fig. 3 displays the nearby galaxy count

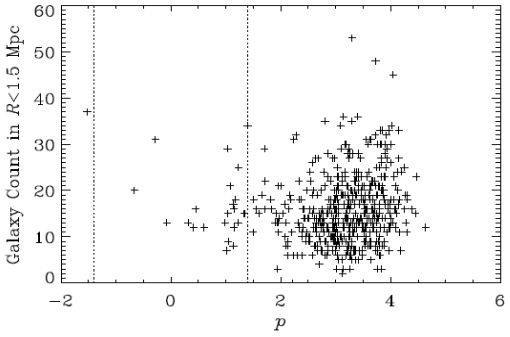

Fig. 2: The radio "loudness" p vs. surrounding galaxy density of QSO2. The radio "loudness" p (see Eq.1) indicates the offset from the best fit line of radio-loud (p=0) sample. The region between the two vertical dotted lines (similar to ±3σ) are expected to be radio-loud objects within the range -1.4 < p < 1.4.

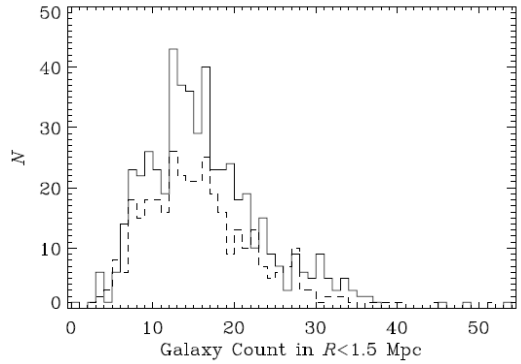

Fig. 3: Nearby galaxy count distribution functions for QSO2 with FIRST detected (solid line) and non-detected (dashed line) subsamples after normalization. These two distributions appear almost identical.

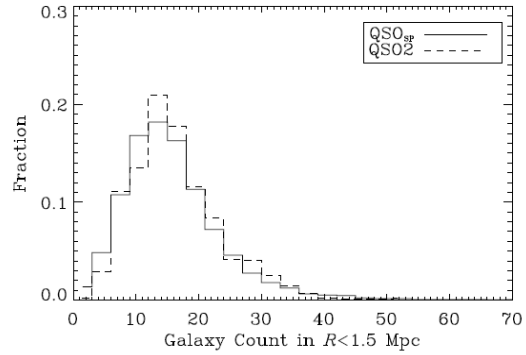

Fig. 4: Comparison of galaxy count distribution functions of QSO2 and QSO_{SP}.

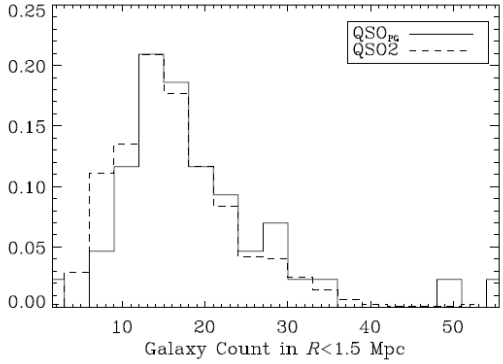

Fig. 5: Galaxy count distribution functions of QSO2 and QSO_{PG}.

distribution functions of QSO2 for FIRST detected and non-detected subsamples, both appear to have an almost identical profile. In addition, we compare the nearby galaxies around spectroscopic quasars (Fig. 4) and PG quasars (Fig. 5) with galaxies around QSO2. The environments of these two QSO1 samples are similar to the QSO2 environment. We also compare the $L_{1.4\mathrm{GHz}}$ vs. galaxy count relation between QSO1 and QSO2 (Fig. 6), both galaxy counts decrease with increasing $L_{1.4\mathrm{GHz}}$. However, the relative *g-i* vs. galaxy count distributions of $\mathrm{QSO_{SP}}$ and QSO2 illustrate an obviously different trend that $\mathrm{QSO_{SP}}$ has a positive slope in Fig. 7 but QSO2 has negative one.

3.3. SDSS color of QSOs

Several authors have suggested the relative SDSS *g-i* color index Δ(*g-i*) (observed *g-i* minus average/median *g-i* of QSOs in the same cosmic epoch) is a useful reddening indicator (Richards et al. 2003; York et al. 2006), and it is adopted in this work to study the dust extinction in photometric quasars, spectroscopic quasars, and QSO2. Figure 8 reveals that Δ(*g-i*) of QSO2 in this work have higher values than that of QSO1 and is consistent with the result in York et al. (2006); on the other hand, the QSO1 Δ(*g-i*)-$L_{1.4\mathrm{GHz}}$ relation is different from the case of QSO2. Figure 9 shows that QSO1 tend to have small Δ(*g-i*) and a negative slope in the Δ(*g-i*) vs. $L_{1.4\mathrm{GHz}}$ plane, whereas QSO2 have higher Δ(*g-i*) and a positive slope in the relation.

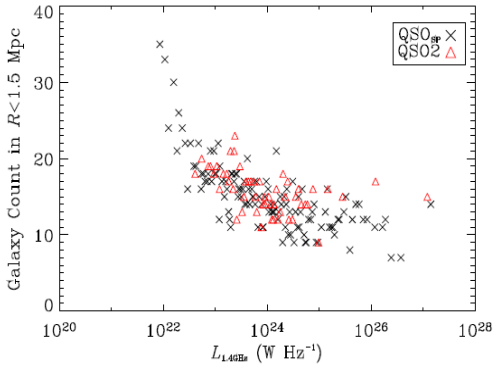

Fig. 6: $L_{1.4\mathrm{GHz}}$ vs. galaxy count of $\mathrm{QSO_{SP}}$ and QSO2. Each data point represents the median value of 10 sources.

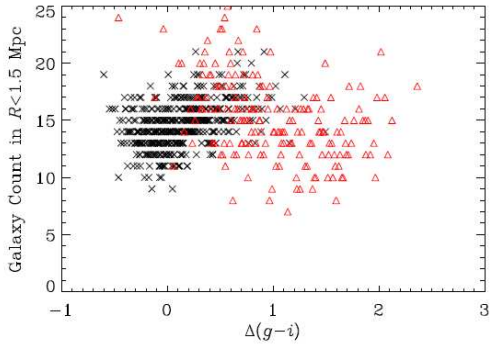

Fig. 7: Δ(*g-i*) vs. galaxy count distribution of $\mathrm{QSO_{SP}}$ (cross symbols) and QSO2 (triangles). Each data point represents the median value of 10 sources.

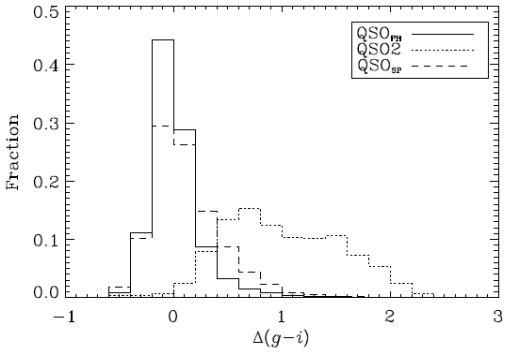

Fig. 8: The Δ(*g-i*) color excess distributions of $\mathrm{QSO_{PH}}$, QSO2, and $\mathrm{QSO_{SP}}$. $\mathrm{QSO_{PH}}$ and $\mathrm{QSO_{SP}}$ have a similar peak value in distribution function at ~ 0.2, whereas QSO2 has a higher relative *g-i* value with peak value ~ 1.

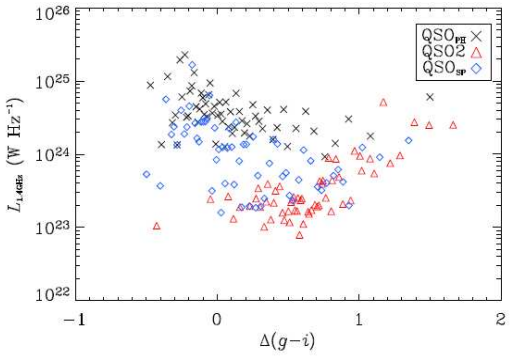

Fig. 9: Correlation between relative *g-i* and $L_{1.4\mathrm{GHz}}$. There is an interesting 'turning point' around relative *g-i* ~ 0.5 where the two variables start to become positively correlated.

3.4. Analysis of Soft X-ray data

Obscuration due to large neutral hydrogen column density is another important issue to study QSO2. We obtain the QSO2 X-ray luminosity from [OIII] luminosity and use the flux limit (Voges et al. 1999) of ROSAT All Sky Survey (RASS) faint/bright source catalogues to estimate the lower limit of neutral hydrogen column density (N_H) of QSO2. First, we convert [OIII] luminosity to intrinsic 2keV soft X-ray luminosity ($L_{2\,keV}$) by the relation (Shen et al. 2006):

$$\log (L_{2keV,\,z=0}) = (0.33 \pm 0.03)(\log L_{[OIII]} - 8.5) + (25.33 \pm 0.02) \quad (2)$$

Then, we calculate 0.1-2.4 keV X-ray luminosity ($L_{0.1\text{-}2.4keV}$) from L_{2keV}, assuming a power-law X-ray spectrum with energy index =1.5 (Shen et al. 2006).

If the central QSO is not obscured by surrounded dust, it may be luminous enough to be seen in soft X-rays, thus we use the flux limit (dashed line in Fig. 10) of RASS (8×10^{-14} erg cm^{-2} s^{-1}, Voges et al. 1999) to estimate at least how much X-ray luminosity is attenuated by neutral hydrogen. Among our QSO2 samples, 786 sources are expected to be detected in RASS at 3 sigma (black dots above the dashed line in Fig.10), and there are126 QSO2 with N_H greater than 10^{22} cm^{-2} (~16%). We also plot the N_H - $\Delta(g\text{-}i)$ relation in Fig. 11, and it shows that N_H is inversely proportional to $\Delta(g\text{-}i)$. Furthermore, we divide all the QSO2 samples into two subgroups based on their $\Delta(g\text{-}i)$ values (see Fig. 12), and study how the source count growing rate changes with different N_H. Most of the QSO2 with lower ($\Delta(g\text{-}i) < 0.6$) have higher N_H greater than 10^{21}cm^{-2}, and the source counts grow sharply between narrow N_H range ($10^{21.5}$ cm^{-2} < N_H < 10^{23} cm^{-2}). In contrary, the cumulative source counts of QSO2 with $\Delta(g\text{-}i) > 0.6$ tend to grow steadily with N_H from 10^{19} cm^{-2} to 10^{23} cm^{-2}. Finally, we use the stacking analysis method to measure the soft X-ray properties of the QSO2, but most of the stacked images are still too faint to provide enough spectroscopic information.

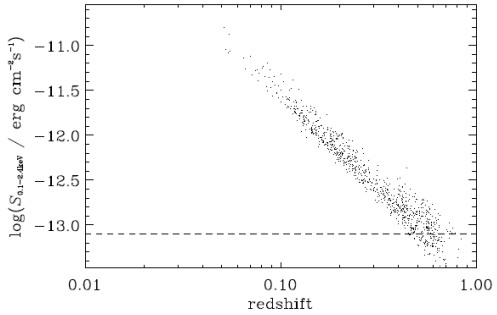

Fig. 10: Flux vs. redshift of QSO2. The black dots are QSO2 with estimated flux L_{2keV} converted from $L_{[OIII]}$ (Shen et al. 2006) and the dashed line is the RASS flux limit (8×10^{-14} erg cm^{-2} s^{-1}). We use this limit to estimate N_H lower limit of QSO2.

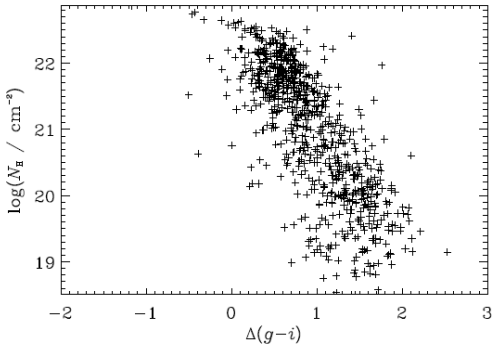

Fig. 11: N_H Lower limit vs. $\Delta(g\text{-}i)$ of QSO2 (cross symbols).

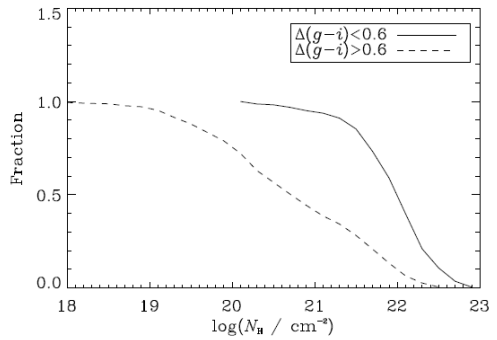

Fig. 12. Source count growing rates in the QSO2 N_H - source count relations for different extinction ranks.

4. Discussion and Conclusion

Although we find no significant difference between the distribution functions of galaxy densities around QSO1 and QSO2 in this work, their relative *g*-*i* values depend differently on the environment. This could suggest the host galaxies of both types of QSOs evolve from galaxies in a similar large scale environment, but some internal characteristic properties make them respond to the external interaction differently, and subsequently result in different dust richness.

The result of radio data analysis further indicates that the dust extinctions are correlated with QSOs radio luminosities at 1.4 GHz (Fig. 9). When compared with QSO1, $L_{1.4\mathrm{GHz}}$ of QSO2 are much weaker by a factor～100, this is consistent with the results of Grimes et al. (2004) and Martínez-Sansigre et al. (2006a). Using L_{151} - $L_{[\mathrm{OIII}]}$ relation, we find 25 out of 531 available QSO2 are radio-loud, and the fraction (~4.7%) is also smaller than that of QSO1 by a factor of about 2 (Green et al. 2009). Hsu & Chen (2010) have shown that the radio properties of these QSO2 are likely powered by AGN, but below radio loudness threshold.

Additional diagnostics of the obscuration in QSO2 is via the column density of neutral hydrogen. Although due to very shallow observations of these QSO2 sources in RASS database, we failed to constrain N_{H} spectroscopically using stacking technique, the no-detection in RASS can still provide lower limits on N_{H} of our QSO2 sources. The lower limits of QSO2 N_{H} derived from SDSS+RASS BSC/FSC show an inversely proportional relation with $\Delta(g\text{-}i)$ and 16% of QSO2 have N_{H} greater than 10^{22} cm^{-2}. This fraction of heavily obscured QSO2 increases significantly when the sample is restricted to QSO2 with small $\Delta(g\text{-}i)$, this indicates a yet unclear underlying connection between the dust and neutral hydrogen in QSO2.

Acknowledgements

Funding for the Sloan Digital Sky Survey (SDSS) and SDSS-II has been provided by the Alfred P. Sloan Foundation, the Participating Institutions, the National Science Foundation, the U.S. Department of Energy, the National Aeronautics and Space Administration, the Japanese Monbukagakusho, Max Planck Society, and the Higher Education Funding Council for England. The SDSS Web site is http://www.sdss.org/.

References

Comastri, A., et al. 1995, *A&A*, 296, 1.

Fiore, F., et al. 2009, *ApJ*, 693, 447.

Gilli, R., et al. 2001, *A&A*, 366, 407.

Grimes, J. A., et al. 2004, *MNRAS*, 349, 503.

Hsu, L. T. & Chen, L.-W. 2010, in preparation.

Jester, S., et al. 2005, *AJ*, 130, 873.

Kewley, L. J., et al. 2001, *ApJ*, 556, 121.

Martínez-Sansigre, A., et al. 2005, *Nature*, 436, 666.

Martínez-Sansigre, A., et al. 2006a, *MNRAS*, 370, 1479.

Martínez-Sansigre, A., et al. 2006b, *MNRAS*, 373, L80.

McCarthy, P. J., 1993, *ARA&A*, 31, 639.

Norman, C., et al. 2002, *ApJ*, 571, 218.

Ofek, E. O., et al. 2007, *MNRAS*, 382, 412.

Reyes, R., et al. 2008, *AJ*, 136, 2373.

Richards, T. A., et al. 2003, *AJ*, 126, 1131.

Poggianti, B. M., et al 2006, *ApJ*, 642, 188.

Ptak, A., et al. 2006, *ApJ*, 637, 147.

Schneider, D. P., et al. 2007, *AJ*, 134, 102.

Shen, S., et al. 2006, *MNRAS*, 369, 1639.

Strand, N. E., et al. 2008, *ApJ*, 688, 180.

Stern, D., et al. 2002, *ApJ*, 568, 71.

Voges, W., et al. 1999, *A&A*, 349, 389.

Wilman, R. J., Fabian, A. C., 1999, *MNRAS*, 309, 862.

Yee, H. K. C. & Ellingson, E., 1993, *ApJ*, 411, 43.

York, D. G., et al. 2006, *MNRAS*, 367, 945.

Zakamska, N. L., et al. 2003, *AJ*, 126, 2125.